

# Scaling the plasma focus for fusion energy considerations

Sor Heoh Saw<sup>1,3</sup> and Sing Lee<sup>1,2,3,\*†</sup>

<sup>1</sup>INTI University College, 71800 Nilai, Malaysia

<sup>2</sup>NSSE, National Institute of Education, Nanyang Technological University, Singapore 637616, Singapore

<sup>3</sup>Institute for Plasma Focus Studies, 32 Oakpark Drive, Chadstone, VIC 3148, Australia

## SUMMARY

Using the Lee model code for dense plasma focus, series of numerical experiments were systematically carried out to determine the scaling of bank energies with total current and focus pinch current and the scaling of neutron yields with energies and currents. The numerical experiments were carried out over a range of bank energies from 8 kJ extending up to 24 MJ on the PF1000 and a proposed less damped modern bank. It also includes a study on the effects of increasing bank energies by increasing bank charging voltage and capacitance of the bank for a practical optimum plasma focus machine. The results provide convincing data to show that it is possible to scale up the plasma focus machine at just 3 MJ for D-D neutron yield of  $10^{13}$  per shot and  $10^{15}$  neutrons per shot when it is converted to operate in D-T. Copyright © 2010 John Wiley & Sons, Ltd.

## KEY WORDS

dense plasma focus; neutrons source; focus pinch current; fusion energy; neutron scaling law

## Correspondence

\*Sing Lee, 32 Oakpark Drive, Chadstone, VIC 3148, Australia.

†E-mail: leeing@optusnet.com.au

Received 16 June 2010; Accepted 19 June 2010

## 1. INTRODUCTION

Plasma focus machines consistently produce considerable amounts of neutrons. The scalability of the device to fusion reactor conditions remains an area of research [1]. Even a simple machine such as the UNU ICTP PFF 3 kJ machine consistently produces  $10^8$  neutrons when operated in deuterium [2]. A big machine such as the PF1000 typically produces  $10^{11}$  neutrons per shot [3]. Gribkov *et al.* [4] had pointed out that  $Y_n = 10^{13}$  in Deuterium is a desired landmark to achieve in a plasma focus device; from the point of view of possible exploitation as a powerful source of fusion neutrons for testing of prospective materials for the first wall components and construction elements in magnetic confinement fusion and also in inertial confinement fusion reactors. Converting such a plasma focus yield to operation in D-T, with  $Y_n = 10^{15}$  could produce, during a 1-year run, an overall fluence-affecting materials to the order of 0.1–1.0 displacements per atom (DPA) (1 DPA is equal to a mean neutron flux of  $4.5 \times 10^{16}$  neutrons  $m^{-2}s^{-1}$  for 1 year) for such testing purposes, at a very low cost relative to

other methods currently being considered. We now examine the requirements to reach this landmark.

This paper presents the results from a series of numerical experiments systematically carried out using the Lee model code [5] to investigate the scalability of the plasma focus to achieve  $Y_n = 10^{13}$  D-D yield. In relation to this, it was necessary to determine the scaling laws between bank energies and peak total current and peak pinch current; and between  $Y_n$  and peak total current and peak pinch current [6–9].

## 2. THE LEE MODEL CODE

### 2.1. Description of the model

The Lee model code couples the electrical circuit with plasma focus dynamics, thermodynamics and radiation, enabling realistic simulation of all gross focus properties. The basic model, described in 1984 [10] was successfully used to assist several projects [11–13]. Radiation-coupled dynamics was included in the five-phase code leading to numerical experiments on

radiation cooling [14]. The vital role of a finite small disturbance speed discussed by Potter in a Z-pinch situation [15] was incorporated together with real gas thermodynamics and radiation-yield terms. Before this ‘communication delay effect’ was incorporated, the model consistently over-estimated the radial speeds. This is serious from the point of view of neutron yields. A factor of 2 in shock speeds gives a factor of 4 in temperatures leading to a difference in fusion cross-sections of  $\sim 1000$  at the range of temperatures we are dealing with. This version of the code assisted other research projects [16–21] and was web-published in 2000 [22] and 2005 [23]. Plasma self-absorption was included in 2007 [22] improving SXR yield simulation. The code has been used extensively in several machines including UNU/ICTP PFF [2,11,16,17,19,20,24,25], NX2 [18,21,26], NX1 [26,27] and adapted for the Filippov-type plasma focus DENA [28]. A recent development is the inclusion of the neutron yield,  $Y_n$ , using a beam-target mechanism [3,6–8,29], incorporated in recent versions [5] of the code (versions later than RADPFV5.13), resulting in realistic  $Y_n$  scaling with  $I_{\text{pinch}}$  [7,8]. The versatility and utility of the model is demonstrated in its clear distinction of  $I_{\text{pinch}}$  from  $I_{\text{peak}}$  [30] and the recent uncovering of a plasma focus pinch current limitation effect [6,29]. The description, theory, code and a broad range of results of this ‘Universal Plasma Focus Laboratory Facility’ are available for download from [5].

## 2.2. A brief description of the code

The five phases are summarized as follows:

1. Axial phase: Described by a snowplow model with an equation of motion coupled to a circuit equation. The equation of motion incorporates the axial phase model parameters: mass and current factors  $f_m$  and  $f_c$ , respectively. The mass swept-up factor  $f_m$  accounts not only for the porosity of the current sheet but also for the inclination of the moving current sheet-shock front structure and all other unspecified effects which have effects equivalent to increasing or reducing the amount of mass in the moving structure, during the axial phase. The current factor,  $f_c$ , accounts for the fraction of current effectively flowing in the moving structure (due to all effects such as current shedding at or near the back-wall and current sheet inclination). This defines the fraction of current effectively driving the structure, during the axial phase.
2. Radial inward shock phase: Described by four coupled equations using an elongating slug model. The first equation computes the radial inward shock speed from the driving magnetic pressure. The second equation computes the axial elongation speed of the column. The third equation computes the speed of the current sheath, also called the magnetic piston, allowing the current sheath to separate from the shock front by applying an adiabatic approximation. The fourth is the circuit equation. Thermodynamic effects due to ionization and excitation are incorporated into these equations, these effects being important for gases other than hydrogen and deuterium. Temperature and number densities are computed during this phase. A communication delay between shock front and current sheath due to the finite small disturbance speed is crucially implemented in this phase. The model parameters, radial phase mass swept-up and current factors,  $f_{mr}$  and  $f_{cr}$ , are incorporated in all three radial phases. The mass swept-up factor  $f_{mr}$  accounts for all mechanisms that have effects equivalent to increasing or reducing the amount of mass in the moving slug, during the radial phase. The current factor,  $f_{cr}$ , accounts for the fraction of current effectively flowing in the moving piston forming the back of the slug (due to all effects). This defines the fraction of current effectively driving the radial slug.
3. Radial reflected shock (RS) phase: When the shock front hits the axis, because the focus plasma is collisional, a RS develops which moves radially outward, whereas the radial current-sheath piston continues to move inward. Four coupled equations are also used to describe this phase, these being for the RS moving radially outward, the piston moving radially inward, the elongation of the annular column and the circuit. The same model parameters,  $f_{mr}$  and  $f_{cr}$ , are used as in the previous radial phase. The plasma temperature behind the RS undergoes a jump by a factor approximately 2.
4. Slow compression (quiescent) or pinch phase: When the out-going RS hits the in-coming piston, the compression enters a radiative phase in which for gases such as neon, radiation emission may actually enhance the compression where we have included energy loss/gain terms from Joule heating and radiation losses into the piston equation of motion. Three coupled equations describe this phase; these being the piston radial motion equation, the pinch column elongation equation and the circuit equation, incorporating the same model parameters as in the previous two phases. Thermodynamic effects are incorporated into this phase. The duration of this slow compression phase is set as the time of transit of small disturbances across the pinched plasma column. The computation of this phase is terminated at the end of this duration.
5. Expanded column phase: To simulate the current trace beyond this point, we allow the column to suddenly attain the radius of the anode and use the expanded column inductance for further integration. In this final phase, the snowplow model is used, and two coupled equations are used; similar to the axial phase aforementioned. This phase is not considered important as it occurs after the focus pinch.

### 2.3. Computation of neutron yield

The neutron yield is computed using a phenomenological beam-target neutron-generating mechanism described recently by Gribkov *et al.* [3] and adapted to yield the following equation. A beam of fast deuteron ions is produced by diode action in a thin layer close to the anode, with plasma disruptions generating the necessary high voltages. The beam interacts with the hot dense plasma of the focus pinch column to produce the fusion neutrons. The beam-target yield is derived [6] as:

$$Y_{b-t} = C_n n_i r_{\text{pinch}}^2 (\ln(b/r_p)) \sigma / U^{0.5} \quad (1)$$

where  $n_i$  is the ion density,  $b$  is the cathode radius,  $r_p$  is the radius of the plasma pinch with length  $z_p$ ,  $\sigma$  the cross-section of the D-D fusion reaction,  $n$ -branch [31] and  $U$ , the beam energy.  $C_n$  is treated as a calibration constant combining various constants in the derivation process.

The D-D cross-section is sensitive to the beam energy in the range 15–150 keV; hence, it is necessary to use the appropriate range of beam energy to compute  $\sigma$ . The code computes induced voltages (due to current motion inductive effects)  $V_{\text{max}}$  of the order of only 15–50 kV. However, it is known from experiments that the ion energy responsible for the beam-target neutrons is in the range 50–150 keV [3], and for smaller lower-voltage machines the relevant energy could be lower at 30–60 keV [24]. Thus, in line with experimental observations the D-D cross-section  $\sigma$  is reasonably obtained by using  $U = 3V_{\text{max}}$ . This fit was tested by using  $U$  equal to various multiples of  $V_{\text{max}}$ . A reasonably good fit of the computed neutron yields to the measured published neutron yields at energy levels from sub-kJ to near MJ was obtained when the multiple of 3 was used; with poor agreement for most of the data points when, for example, a multiple of 1 or 2 or 4 or 5 was used. The model uses a value of  $C_n = 2.7 \times 10^7$  obtained by calibrating the yield [5,6] at an experimental point of 0.5 MA.

The thermonuclear component is also computed in every case and it is found that this component is negligible when compared with the beam-target component.

## 3. PROCEDURES FOR NUMERICAL EXPERIMENTS

The Lee model code is configured to work as any plasma focus by inputting the bank parameters,  $L_0$ ,  $C_0$  and stray circuit resistance  $r_0$ ; the tube parameters  $b$ ,  $a$  and  $z_0$  and operational parameters  $V_0$  and  $P_0$  and the fill gas. The standard practice is to fit the computed total current waveform to an experimentally measured total current waveform [5–8,23,24,29,30] using four model parameters representing the mass swept-up

factor  $f_m$ , the plasma current factor  $f_c$  for the axial phase and factors  $f_{mr}$  and  $f_{cr}$  for the radial phases.

From experience, it is known that the current trace of the focus is one of the best indicators of gross performance. The axial and radial phase dynamics and the crucial energy transfer into the focus pinch are among the important information that is quickly apparent from the current trace.

The exact time profile of the total current trace is governed by the bank parameters, by the focus tube geometry and the operational parameters. It also depends on the fraction of mass swept-up and the fraction of sheath current and the variation of these fractions through the axial and radial phases. These parameters determine the axial and radial dynamics, specifically the axial and radial speeds which in turn affect the profile and magnitudes of the discharge current. The detailed profile of the discharge current during the pinch phase also reflects the Joule heating and radiative yields. At the end of the pinch phase, the total current profile also reflects the sudden transition of the current flow from a constricted pinch to a large column flow. Thus the discharge current powers all dynamic, electrodynamic, thermodynamic and radiation processes in the various phases of the plasma focus. Conversely, all the dynamic, electrodynamic, thermodynamic and radiation processes in the various phases of the plasma focus affect the discharge current. It is then no exaggeration to say that the discharge current waveform contains information on all the dynamic, electrodynamic, thermodynamic and radiation processes that occur in the various phases of the plasma focus. This explains the importance attached to matching the computed current trace to the measured current trace in the procedure adopted by the Lee model code.

For this series of experiments, we configure the Lee model code using a published current trace measured from the PF1000 with  $C_0 = 1332 \mu\text{F}$ , operated at 27 kV, 3.5 torr deuterium, with cathode/anode radii  $b = 16 \text{ cm}$ ,  $a = 11.55 \text{ cm}$  and anode length  $z_0 = 60 \text{ cm}$  [3]. In the numerical experiments, we fitted external (or static) inductance  $L_0 = 33.5 \text{ nH}$  and stray resistance  $r_0 = 6.1 \text{ m}\Omega$  (damping factor  $\text{RESF} = \text{stray resistance} / (L_0/C_0)^{0.5} = 1.22$ ). The fitted model parameters are  $f_m = 0.13$ ,  $f_c = 0.7$ ,  $f_{mr} = 0.35$  and  $f_{cr} = 0.65$ . Figure 1 shows the computed current trace [5,6,29] agreeing very well with the measured trace through all the phases, axial and radial, right down to the bottom of the current dip indicating the end of the pinch phase. This agreement confirms the model parameters for the PF1000. Once the model parameters have been fitted to a machine for a given gas, these model parameters may be used with some degree of confidence when operating parameters such as the voltage are varied [5]. With no measured current waveform available for the higher megajoule numerical experiments, it is reasonable to keep the model parameters that we have got from the PF1000 fitting.

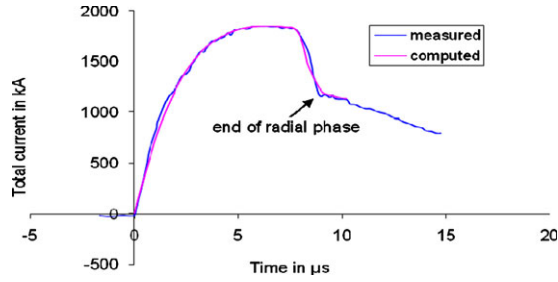


**Figure 1.** Fitting computed current trace to measured current trace to obtain fitted parameters  $f_m = 0.13$ ,  $f_c = 0.7$ ,  $f_{mr} = 0.35$  and  $f_{cr} = 0.65$ . In this example for PF1000, the fitting is found to be good for the phases up to the end of the radial phase.

### 3.1. Determining the scaling laws for neutrons from numerical experiments over a range of energies from 8.5 kJ to 24.5 MJ

Using the model parameters determined in the above for PF1000, we run the first series of numerical experiments on PF1000-like machines at  $V_0 = 35$  kV,  $P_0 = 10$  torr,  $L_0 = 33.5$  nH,  $RESF = 1.22$  and the  $c = b/a = 1.39$  for varying bank energies from 8.5 kJ to 24.5 MJ. This series of numerical experiments is operated at optimum pressure of 10 torr deuterium, and the ratio  $b/c$  retained at 1.39.

The numerical experiments were carried out for  $C_0$  ranging from 14 to 39 960  $\mu$ F corresponding to energies from 8.5 kJ to 24.5 MJ. For each  $C_0$ , we parametrically varied  $z_0$  and then ‘ $a$ ’ to find the optimum combination of  $z_0$  and ‘ $a$ ’ for each given  $C_0$  corresponding to an end axial speed of 10 cm/ $\mu$ s. The optimum combinations for each  $C_0$  are summarized in Table I together with the peak total current, peak pinch current and neutron yield computed for the range of bank energies from 8.5 kJ to 24.5 MJ.

The results show no saturation of the peak total current and peak pinch current as the energies of the bank is increased. However, it is clear that the scaling deteriorates with increasing bank energies.

Figure 2 shows the computed  $I_{peak}$  as a function of  $C_0$ , which shows no saturation; although there is a scaling shift from  $I_{peak} \sim E_0^{0.41}$  to  $I_{peak} \sim E_0^{0.22}$  which is seen when plotted on log–log scale (Figure 3).

Similarly, the  $I_{pinch}$  scaling with  $E_0$  slows down from  $I_{pinch} \sim E_0^{0.41}$  to  $I_{pinch} \sim E_0^{0.22}$  (Figure 3), but again no saturation. We would like to emphasize that the findings in earlier papers [6,7,29,30] concluded that it is the  $I_{pinch}$  scaling, rather than  $I_{peak}$  which directly affects the neutron yield scaling.

For this series of experiments, we find that the  $Y_n$  scaling decreases from  $Y_n \sim E_0^{2.0}$  at tens of kJ to  $Y_n \sim E_0^{0.84}$  at the highest energies (up to 24.5 MJ). This is shown in Figure 4.

Because of the way  $Y_n$  versus  $E_0$  scaling slows down at the megajoule level and the corresponding way  $I_{peak}$

**Table I.** Numerical experiments to find the scaling of  $I_{peak}$ ,  $I_{pinch}$  and  $Y_n$  with  $C_0$ .

| $E_0$ (kJ) | $C_0$ ( $\mu$ F) | $a$ (cm) | $z_0$ (cm) | $I_{peak}$ (kA) | $I_{pinch}$ (kA) | $Y_n$ ( $10^{10}$ ) |
|------------|------------------|----------|------------|-----------------|------------------|---------------------|
| 24 476     | 39 960           | 23.55    | 500.0      | 5678            | 2368             | 1320                |
| 18 765     | 30 636           | 22.80    | 400.0      | 5479            | 2267             | 1094                |
| 14 685     | 23 976           | 21.90    | 350.0      | 5268            | 2165             | 906                 |
| 11 422     | 18 648           | 21.00    | 300.0      | 5046            | 2062             | 737                 |
| 6527       | 10 656           | 18.73    | 220.0      | 4506            | 1827             | 438                 |
| 4895       | 7992             | 17.66    | 160.0      | 4229            | 1721             | 329                 |
| 4079       | 6660             | 16.88    | 140.0      | 4043            | 1650             | 273                 |
| 3263       | 5328             | 15.90    | 120.0      | 3812            | 1563             | 215                 |
| 2448       | 3996             | 14.53    | 86.6       | 3510            | 1461             | 159                 |
| 1632       | 2664             | 12.69    | 65.0       | 3101            | 1316             | 102                 |
| 816        | 1332             | 9.95     | 45.0       | 2458            | 1086             | 45.4                |
| 748        | 1221             | 9.62     | 42.0       | 2383            | 1059             | 40.9                |
| 680        | 1110             | 9.18     | 38.0       | 2295            | 1032             | 36.3                |
| 612        | 999              | 8.82     | 36.0       | 2208            | 1000             | 31.8                |
| 544        | 888              | 8.47     | 35.0       | 2116            | 965              | 27.3                |
| 476        | 777              | 8.05     | 33.0       | 2012            | 926              | 22.9                |
| 408        | 666              | 7.60     | 31.0       | 1898            | 882              | 18.6                |
| 340        | 555              | 7.04     | 28.0       | 1766            | 833              | 14.5                |
| 272        | 444              | 6.38     | 24.0       | 1613            | 778              | 10.8                |
| 204        | 333              | 5.59     | 20.0       | 1425            | 706              | 7.1                 |
| 136        | 222              | 4.74     | 17.0       | 1205            | 613              | 3.8                 |
| 68         | 111              | 3.47     | 12.0       | 888             | 476              | 1.21                |
| 34         | 56               | 2.48     | 8.0        | 644             | 363              | 0.346               |
| 17         | 28               | 1.72     | 5.0        | 457             | 272              | 0.085               |
| 8.5        | 14               | 1.28     | 4.0        | 335             | 202              | 0.017               |

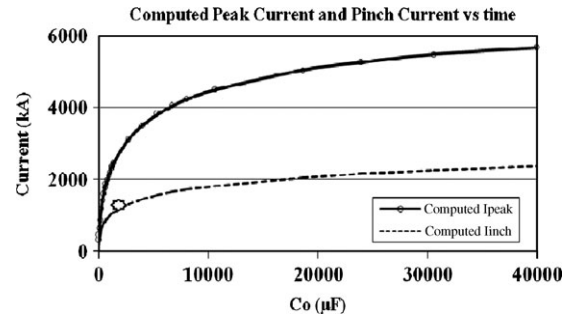


**Figure 2.**  $I_{peak}$  (top trace) computed from numerical experiments as a function of  $C_0$ . Also shown is the  $I_{pinch}$  curve (lower trace). The single point at the 2 MA level is an experimental PF1000 point.

and  $I_{pinch}$  scaling with  $E_0$  also slow down, the scaling of  $Y_n$  with  $I_{peak}$  and  $I_{pinch}$  over the whole range of energies investigated up to 24.5 MJ (Figure 5) are as follows:

$$Y_n = 3.2 \times 10^{11} I_{pinch}^{4.5};$$

$$Y_n = 1.8 \times 10^{10} I_{peak}^{3.8} \text{ where } I_{pinch} (0.2 - 2.4) \text{ and } I_{peak} (0.3 - 5.7) \text{ are in MA.}$$

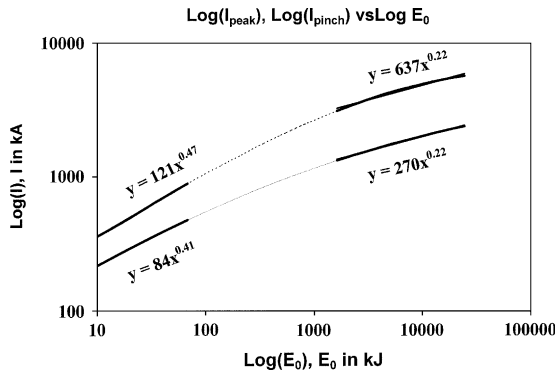


**Figure 3.** Log  $I_{\text{peak}}$  (top curve) and Log  $I_{\text{pinch}}$  versus Log  $E_0$ , showing no saturation for  $E_0$  up to 24.5 MJ.

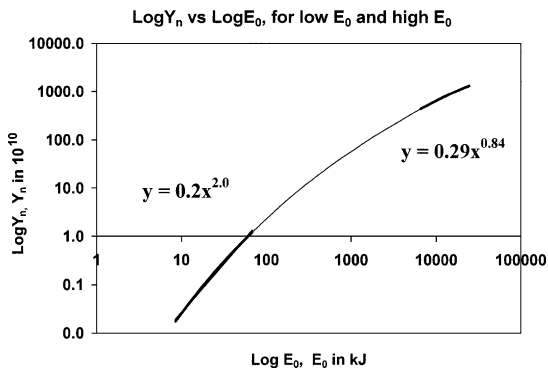


**Figure 4.**  $Y_n$  plotted as a function of  $E_0$  in log–log scale, showing no saturation of neutron yield up to 24.5 MJ, the highest energy investigated.

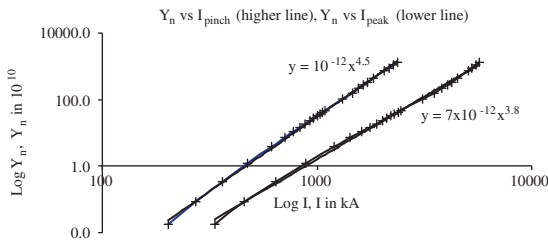


**Figure 5.** Log( $Y_n$ ) scaling with Log( $I_{\text{peak}}$ ) and Log( $I_{\text{pinch}}$ ), for the range of energies investigated, up to 24.5 MJ.

In the above series of numerical experiments, we have shown that as the bank energies of the plasma focus increase from 10 kJ to 25 MJ:

$$I_{\text{peak}} \sim E_0^x \text{ where } x = 0.47 \text{ at tens of kJ and } x = 0.22 \text{ at the highest energies (up to 24.5 MJ)}$$

$$I_{\text{pinch}} \sim E_0^x \text{ where } x = 0.41 \text{ at tens of kJ and } x = 0.22 \text{ at the highest energies (up to 24.5 MJ)}$$

$$Y_n \sim E_0^x, \text{ where } x = 2.0 \text{ at tens of kJ and } x = 0.84 \text{ at the highest energies (up to 24.5 MJ)}$$

$Y_n$  does not saturate with increasing  $E_0$  at the megajoule level and the resultant scaling laws for  $Y_n$  in relation to the total peak current,  $I_{\text{peak}}$  and the total pinch current  $I_{\text{pinch}}$  are

$$Y_n = 3.2 \times 10^{11} I_{\text{pinch}}^{4.5} \text{ where } I_{\text{pinch}} (0.2 - 2.4) \text{ in MA;}$$

and

$$Y_n = 1.8 \times 10^{10} I_{\text{peak}}^{3.8} \text{ where } I_{\text{peak}} (0.3 - 5.7) \text{ in MA}$$

This series of numerical experiments show that it is possible to scale up the plasma focus machine to a yield of  $10^{13}$  D-D neutrons. This is achieved at bank energy  $E_0 = 18.7$  MJ with  $I_{\text{peak}} = 5.5$  MA and  $I_{\text{pinch}} = 2.3$  MA, corresponding to the focus anode length  $z_0 = 4$  m and anode radius  $a = 22.8$  cm and cathode radius  $b = 31.7$  cm.

### 3.2. Investigating the effect of RESF on $Y_n$ yield

The PF1000 has an unusually high damping factor represented by RESF = 1.22. As it is practically possible for a modern capacitor bank system to be very much less damped with RESF = 0.12, we proceed to run the second series of numerical experiments with RESF changed to 0.12. Again for each  $C_0$ , we parametrically varied  $z_0$  and then ‘ $a$ ’ to find the optimum combination of  $z_0$  and ‘ $a$ ’ for each given  $C_0$  corresponding to an end axial speed of 10 cm/ $\mu$ s. The optimum combinations for each  $C_0$  and with the peak total current, peak pinch current and neutron yield computed for the range of bank energies from 68 kJ to 24.5 MJ are tabulated in Table II. Figure 6 shows the summary of the results.

These results show that using a less resistive modern bank, RESF = 0.12 reduces the  $E_0$  required to reach  $Y_n = 10^{13}$  in Deuterium to some 8 MJ with corresponding  $I_{\text{peak}} = 6$  MA,  $I_{\text{pinch}} = 2.3$  MA, the focus length  $z_0 = 2.6$  m, anode radius  $a = 25.3$  cm and cathode radius  $b = 35.2$  cm; as compared with 19 MJ with corresponding  $I_{\text{peak}} = 5.5$  MA,  $I_{\text{pinch}} = 2.3$  MA, the focus length  $z_0 = 4$  m, anode radius  $a = 22.8$  cm and cathode radius  $b = 31.7$  cm for the earlier heavily damped bank with RESF = 1.22.

### 3.3. Investigating the effect on $Y_n$ as operating voltage is increased from 35 to 90 kV, at $C_0 = 777 \mu\text{F}$

We run a third series of numerical experiments for a practical optimum configuration [8] with  $c = b/a = 1.39$ ,  $L_0 = 36$  nH,  $P_0 = 10$  torr and  $C_0 = 777 \mu\text{F}$ , and vary  $V_0$  from 35 to 90 kV. The results are summarized in Table III and plotted in Figure 7 in log–log scale.

Figure 7 shows that  $Y_n \sim V_0^{2.8}$  over the range of voltages examined from 35 to 90 kV. Looking at this scaling, it may at first sight be tempting to think in terms of increasing the voltage further. However, it is then necessary to look more closely at that prospect.

**Table II.** Numerical experiments with less resistive bank of RESF = 0.12.

| $E_0$ (kJ) | $C_0$ ( $\mu$ F) | $a$ (cm) | $z_0$ (cm) | $I_{peak}$ (kA) | $I_{pinch}$ (kA) | $Y_n$ ( $10^{10}$ ) |
|------------|------------------|----------|------------|-----------------|------------------|---------------------|
| 24 476     | 39 960           | 28.25    | 450.0      | 6774            | 2720             | 2255                |
| 18 765     | 30 636           | 27.44    | 430.0      | 6612            | 2622             | 1968                |
| 14 685     | 23 976           | 27.01    | 350.0      | 6488            | 2541             | 1711                |
| 11 421     | 18 646           | 26.34    | 300.0      | 6327            | 2449             | 1460                |
| 8159       | 13 320           | 25.26    | 260.0      | 6077            | 2314             | 1157                |
| 6527       | 10 656           | 24.62    | 210.0      | 5909            | 2236             | 974                 |
| 4895       | 7992             | 23.61    | 160.0      | 5663            | 2130             | 777                 |
| 4079       | 6660             | 22.83    | 140.0      | 5487            | 2060             | 668                 |
| 3263       | 5328             | 21.72    | 110.0      | 5252            | 1976             | 558                 |
| 2448       | 3996             | 20.36    | 93.0       | 4948            | 1866             | 437                 |
| 1632       | 2664             | 18.40    | 75.0       | 4512            | 1711             | 303                 |
| 816        | 1332             | 14.74    | 47.0       | 3726            | 1466             | 154                 |
| 748        | 1221             | 14.26    | 44.0       | 3623            | 1436             | 140                 |
| 680        | 1110             | 13.90    | 43.0       | 3528            | 1402             | 127                 |
| 612        | 999              | 13.46    | 41.0       | 3419            | 1366             | 113                 |
| 476        | 777              | 12.42    | 37.0       | 3161            | 1280             | 85.72               |
| 340        | 555              | 10.61    | 28.0       | 2763            | 1175             | 58.43               |
| 204        | 333              | 8.81     | 22.0       | 2312            | 1025             | 32.30               |
| 136        | 222              | 7.33     | 17.0       | 1954            | 913              | 19.46               |
| 68         | 111              | 5.45     | 12.0       | 1472            | 735              | 7.64                |

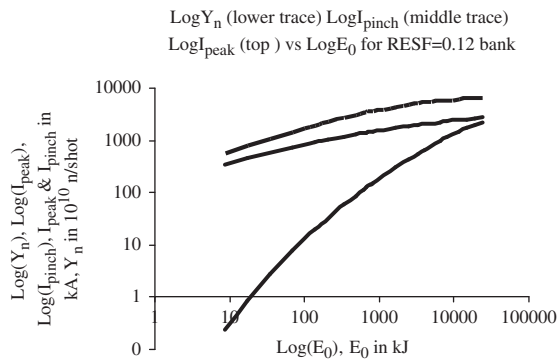


**Figure 6.** Log-log plots of  $Y_n$  (lower trace),  $I_{pinch}$  (middle trace) and  $I_{peak}$  (top trace) versus  $E_0$  for a high-performance bank up to 25MJ; computed from numerical experiments.

**Table III.** Numerical experiments on effect of increasing  $V_0$ , at fixed  $C_0$  of 777  $\mu$ F.

| $V_0$ (kV) | $E_0$ (kJ) | $b$ (cm) | $a$ (cm) | $z_0$ (cm) | $I_{peak}$ (kA) | $I_{pinch}$ (kA) | $Y_n$ ( $10^{10}$ ) |
|------------|------------|----------|----------|------------|-----------------|------------------|---------------------|
| 90         | 3147       | 39.92    | 27.65    | 25         | 7580            | 2483             | 1228                |
| 70         | 1904       | 31.14    | 22.40    | 30         | 5955            | 2091             | 631                 |
| 50         | 971        | 23.44    | 16.86    | 35         | 4365            | 1652             | 246                 |
| 35         | 476        | 16.69    | 12.01    | 37         | 3074            | 1286             | 88                  |

An examination of the computed results shows that the computed effective beam energy [6,7,29] for 90 kV is already at the 330 keV level. Looking at data for the

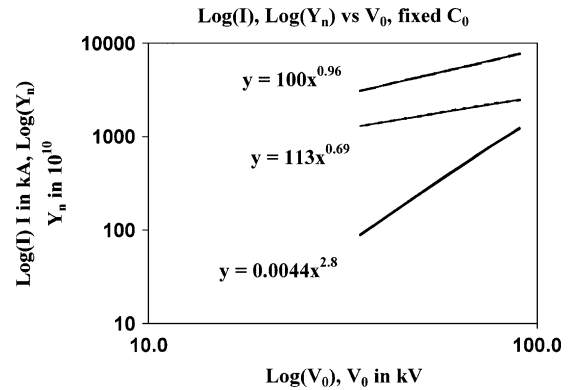


**Figure 7.** Scaling of currents and  $Y_n$  as functions of operating voltage  $V_0$ . Top curve:  $\text{Log}(I_{peak})$ , middle curve:  $\text{Log}(I_{pinch})$  and bottom curve:  $\text{Log}(Y_n)$ .

D-D cross-section [31] as a function of beam energy, it is seen that above 300 keV, the rise in D-D fusion cross-section is very slow. Hence, we wish to highlight that there is little advantage operating above 90 kV. In fact, the situation is actually disadvantageous to increase operating voltage if one considers changing to D-T operation. The D-T fusion cross-section [31] has already peaked at 120 keV; and operating at 90 kV with the beam energy at 330 keV, the beam energy is already too high; the D-T cross-section having dropped by a factor around 3.6 from its peak. It seems then that from this point of view there is no advantage to operate a plasma focus at higher than 90 kV. For conversion to D-T operation, it would probably be better to operate at a lower voltage. It would then be necessary to increase  $C_0$  until  $10^{15}$  D-T neutrons is reached.

### 3.4. Investigating operation at 90 kV, varying $E_0$ by varying $C_0$ ; at 10 torr, $L_0 = 36$ nH, and $b/a = 1.39$ ; RESF = 0.12

We consider the effect of operating at 90 kV. We run the fourth series of numerical experiments at 90 kV with increasing  $E_0$  (by increasing  $C_0$ ) to obtain the energy required to reach  $Y_n = 10^{13}$  D-D neutrons per shot. At each  $C_0$ ,  $z_0$  is varied while adjusting 'a' for an end axial speed of 10 cm/ $\mu$ s. The optimum  $z_0$  is thus found for each  $C_0$ . Results are shown in Figure 8. Again at this higher voltage, no saturation is found for  $I_{peak}$ ,  $I_{pinch}$  or  $Y_n$ . At 90 kV, the results show that the  $E_0$  required for  $Y_n = 10^{13}$  D-D fusion neutrons per shot is reduced further to 3 MJ, with  $C_0 = 777 \mu$ F as shown in Figure 8. The values of  $I_{peak}$  and  $I_{pinch}$  are 7.6 and 2.5 MA, respectively. Furthermore, at 90 kV with the highest value of  $C_0$  investigated as 39 960  $\mu$ F, the storage energy is 162 MJ. At that storage energy, optimized  $Y_n$  is  $4.5 \times 10^{14}$  D-D neutrons/shot with  $I_{peak} = 17.3$  MA and  $I_{pinch} = 5.7$  MA.

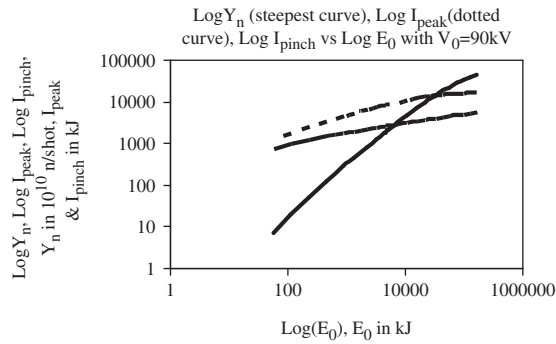


**Figure 8.** Numerical experiments at 90 kV, varying  $C_0$ , to obtain scaling of  $I_{\text{peak}}$ ,  $I_{\text{pinch}}$  and  $Y_n$  with  $E_0$ .  $\text{Log}(Y_n)$ , steepest curve;  $\text{Log}(I_{\text{peak}})$ , dotted curve;  $\text{Log}(I_{\text{pinch}})$ , other curve.  $Y_n$  in units of  $10^{10}$  D-D neutrons/shot;  $I_{\text{peak}}$  and  $I_{\text{pinch}}$  in kA.

#### 4. CONCLUSIONS

This paper finds that it is possible to scale up the focus to useful fusion conditions. In the first series of numerical experiments, we have shown that as the bank energies of the plasma focus increase from 10 kJ to 25 MJ:

$$I_{\text{peak}} \sim E_0^x \text{ where } x = 4.7 \text{ at tens of kJ and } x = 0.22 \text{ at the highest energies (up to 25 MJ)}$$

$$I_{\text{pinch}} \sim E_0^x \text{ where } x = 4.1 \text{ at tens of kJ and } x = 0.22 \text{ at the highest energies (up to 25 MJ)}$$

$$Y_n \sim E_0^x, \text{ where } x = 2.0 \text{ at tens of kJ and } x = 0.84 \text{ at the highest energies (up to 25 MJ)}$$

$Y_n$  does not saturate with increasing  $E_0$  at the megajoule level and the resultant scaling laws for  $Y_n$  in relation to the total peak current,  $I_{\text{peak}}$  and the total pinch current  $I_{\text{pinch}}$  are

$$Y_n = 3.2 \times 10^{11} I_{\text{pinch}}^{4.5} \text{ where } I_{\text{pinch}} (0.2 - 2.4) \text{ in MA}$$

$$Y_n = 1.8 \times 10^{10} I_{\text{peak}}^{3.8} \text{ where } I_{\text{peak}} (0.3 - 5.7) \text{ in MA}$$

To scale up from a PF1000-like capacitor bank requires close to 19 MJ to reach a target D-D neutron yield of  $10^{13}$  per shot, this level of neutron yield being a desired landmark to achieve in a plasma focus device; from the point of view of possible exploitation as a powerful source of fusion neutrons for testing of prospective fusion reactor wall materials. The energy requirement can be reduced to 8 MJ using a modern capacitor bank with typical lower damping operating at typical voltage of 35 kV. By increasing the operational voltage to 90 kV, the energy requirement is further reduced to 3 MJ. Because of the high-effective beam energy already at 90 kV, there is little advantage to operate at voltages above 90 kV for D-D neutron yield, from the point of view of fusion cross-section.

#### REFERENCES

- Haines MG. In *Laser and Plasma Technology*, Lee S, Tan BC, Wong CS, Chew AC (eds). World Scientific: Singapore, 1985; 560–585.
- Lee S. Twelve Years of UNU/ICTP PFF—A Review, IC/98/231 Abdus Salam ICTP, Miramare, Trieste; 1998, pp.5–34. ICTP Open Access Archive <http://eprints.ictp.it/31/>.
- Gribkov VA, Banaszak A, Bienkowska B, Dubrovsky AV, Ivanova-Stanik I, Jakubowski L, Karpinski L, Miklaszewski RA, Paduch M, Sadowski MJ, Scholz M, Szydowski A, Tomaszewski K. Plasma dynamics in the PF-1000 device under full-scale energy storage: II. Fast electron and ion characteristics versus neutron emission parameters and gun optimization perspectives. *Journal of Physics D-Applied Physics* 2007; **40**:3592–3607.
- Gribkov VA *et al.* Plasma dynamics in PF-1000 device under full-scale energy storage: I pinch dynamics, shock wave diffraction, and inertial electrode. *Journal of Physica D-Applied Physics* 2007; **40**:1977–1989.
- Lee S. Radiative Dense Plasma Focus Computation Package: RADPF. Available from: <http://www.intimal.edu.my/school/fas/UFLF/File1RADPF.htm> <http://www.plasmafocus.net/IPFS/modelpackage/File1RADPF.htm>.
- Lee S, Saw SH. Pinch current limitation effect in plasma focus. *Applied Physics Letters* 2008; **92**: 021503.
- Lee S, Saw SH. Neutron scaling laws from numerical experiments. *Journal of Fusion Energy* 2008; **27**:292–295.
- Lee S. Current and neutron scaling for megajoule plasma focus machine. *Plasma Physics and Controlled Fusion* 2008; **50**(14):105005.
- Lee S, Saw SH, Soto L, Springham SV, Moo SP. Numerical experiments on plasma focus neutron yield versus pressure compared with laboratory experiments. *Plasma Physics and Controlled Fusion* 2009; **51**(11):075006.
- Lee S. Plasma focus model yielding trajectory and structure. In *Radiations in Plasmas*, vol. II, McNamara B (ed.). World Scientific Publishing Co: Singapore, 1984; 978–987. ISBN 9971-966-37-9.
- Lee SS *et al.* A simple facility for the teaching of plasma dynamics and plasma nuclear fusion. *American Journal of Physics* 1988; **56**:62–68.
- Tou TY, Lee S, Kwek KH. Non perturbing plasma focus measurements in the run-down phase. *IEEE Transactions on Plasma Science* 1989; **17**:311–315.

13. Lee S. A sequential plasma focus. *IEEE Transactions on Plasma Science* 1991; **19**(12):912–919.
14. Bin Ali J. Development and studies of a small plasma focus. *Ph.D. Thesis*, Universiti Teknologi Malaysia, Malaysia, 1990.
15. Potter DE. The formation of high-density z-pinch. *Nuclear Fusion* 1978; **18**:813–823.
16. Lee S, Serban AA. Dimensions and lifetime of the plasma focus pinch. *IEEE Transactions on Plasma Science* 1996; **24**(3):1101–1105.
17. Mahe L. Soft X-rays from compact plasma focus. *Ph.D. Thesis*, NIE, Nanyang Technological University, Singapore, 2006. ICTP Open Access Archive: <http://eprints.ictp.it/327/>.
18. Bing S. Plasma dynamics and x-ray emission of the plasma focus. *Ph.D. Thesis*, NIE, Nanyang Technological University, Singapore, 2000. ICTP Open Access Archive: <http://eprints.ictp.it/99/>.
19. Serban A, Lee S. Experiments on speed-enhanced neutron yield from a small plasma focus. *Journal of Plasma Physics* 1998; **60**(part 1):3–15.
20. Liu MH, Feng XP, Springham SV, Lee S. Soft x-ray measurement in a small plasma focus operated in neon. *IEEE Transactions on Plasma Science* 1998; **26**:135–140.
21. Wong D, Lee P, Zhang T, Patran A, Tan TL, Rawat RS, Lee S. An improved radiative plasma focus model calibrated for neon-filled NX2 using a tapered anode. *Plasma Sources Science Technology* 2007; **16**:116–123.
22. Lee S. 2000–2007. Available from: <http://ckplee.myplace.nie.edu.sg/plasmaphysics/>.
23. Lee S. 2005. ICTP Open Access Archive: <http://eprints.ictp.it/85/>.
24. Springham SV, Lee S, Rafique MS. Correlated deuteron energy spectra and neutron yield for a 3 kJ plasma focus. *Plasma Physics and Controlled Fusion* 2000; **24**:1023–1032.
25. Mohammadi MA, Sobhanian S, Wong CS, Lee S, Lee P, Rawat RS. The effect of anode shape on neon soft x-ray emissions and current sheath configuration in plasma focus device. *Journal of Physics D-Applied Physics* 2009; **42**:045203 (10).
26. Lee S, Lee P, Zhang G, Feng X, Gribkov VA, Mahe L, Serban A, Wong TKS. High rep rate, high performance plasma focus as a powerful radiation source. *IEEE Transactions on Plasma Science* 1998; **26**:119.
27. Bogolyubov EP, Bochkov VD, Veretennikov VA, Vekhoreva LT, Gribkov VA, Dubrovskii AV, Ivanov YuP, Isakov AI, Krokhin ON, Lee P, Lee S, Nikulin VYa, Serban A, Silin PV, Feng X, Zhang GX. A powerful soft x-ray source for x-ray lithography based on plasma focusing. *Physica Scripta* 1998; **57**:488–494.
28. Siahpoush V, Tafreshi MA, Sobhanian S, Khorram S. Adaptation of Sing Lee's model to the Filippov type plasma focus geometry. *Plasma Physics and Controlled Fusion* 2005; **47**:1065–1072.
29. Lee S, Lee P, Saw SH, Rawat RS. Numerical experiments on plasma focus pinch current limitation. *Plasma Physics and Controlled Fusion* 2008; **50**:065012 (8).
30. Lee S, Saw SH, Lee PCK, Rawat RS, Schmidt H. Computing plasma focus pinch current from total current measurement. *Applied Physics Letters* 2008; **92**:111501.
31. Huba JD. Plasma Formulary pg44. 2006. Available from: [http://wwwppd.nrl.navy.mil/nrlformulary/NRL\\_FORMULARY\\_07.pdf](http://wwwppd.nrl.navy.mil/nrlformulary/NRL_FORMULARY_07.pdf).